Evolution of the fishtail-effect in pure and Ag-doped MG-YBCO

D. A. Lotnyk,* R. V. Vovk, M. A. Obolenskii, and A. A. Zavgorodniy
Physical department, V.N. Karazin Kharkov National University, 4 Svoboda Square, 61077 Kharkov, Ukraine.

J. Kováč, V. Antal, M. Kaňuchová, M. Šefčiková, and P. Diko
Materials Physics Laboratory, Institute of Experimental Physics, Slovak Academy of Sciences, Watsonova 47, 04001 Košice, Slovakia

A. Feher
Centre of Low Temperature Physics, Faculty of science, P.J. Šafarik University, Park Angelinum 9, 041 54 Košice, Slovakia

A. Chroneos
Department of Materials, Imperial College, London SW7 2AZ, United Kingdom
(Dated: June 24, 2010)

We report on magnetic measurements carried out in a textured $YBa_2Cu_3O_{7-\delta}$ and $YBa_2(Cu_{1-x}Ag_x)_3O_{7-\delta}$ (at $x \approx 0.02$) crystals. The so-called fishtail-effect (FE) or second magnetization peak has been observed in a wide temperature range $0.4 < T/T_c < 0.8$ for $\mathbf{H} \parallel c$. The origin of the FE arises for the competition between surface barrier and bulk pinning. This is confirmed in a non-monotonically behavior of the relaxation rate R. The value H_{max} for Ag-doped crystals is larger than for the pure one due to the presence of additional pinning centers, above all on silver atoms.

PACS numbers: 74.25.Qt, 74.72.Bk, 74.81.Bd
Keywords: Textured-YBCO, fishtail effect, bulk pinning, surface barriers

I. INTRODUCTION

Since the discovery of high-temperature superconductors (HTSCs), their engineering applications at liquid nitrogen temperatures have drawn much attention. The $YBa_2Cu_3O_{7-\delta}$ (YBCO) is one of the promising HTSCs materials for various technical applications. However, in ceramic materials the critical current density (J_c) is, due to the weak link effects, very low, rendering them unsuitable for applications. In order to enhance J_c, the so-called melt-textured growth (MG) process [1] has been developed, which can significantly enhance J_c. One interesting phenomenon in the MG HTSCs is the fishtail effect (FE) in J_c as well as in isothermal magnetic hysteresis loops [2–4]. As for the FE origin, some researchers propose the vortex ordered phase to disordered phase transition [5–7] to explain this interesting phenomenon, while others attribute it to the bulk pinning [2–4]. In the vortex phase transition explanation, the FE exists both on a single $J_c(T)$ curve and on a single $J_c(H)$ curve. However, in the bulk pinning explanation, the FE appears on $M(H)$ curves whereas on a single magnetization vs. temperature curve it is seldom reported. In the previous work, the critical state model was used to study the isothermal $M(H)$ curves [8]. However, for HTSCs, due to their operation at higher temperatures and due to their small activation energy U, the flux creep is significant. Hence, non-linear flux creep models were developed. Meanwhile, the surface barrier [9], which prevents vortex entering (which characterized by magnetic field H_{en}) and exiting (H_{ex}) superconductors, has strong effects on the irreversibility of HTSCs. In [10] it was pointed out that in the case of a competition between bulk and surface pinning, the initial relaxation is determined by the smaller pinning energy between U_{bulk} and $U_{surface}$. Thus, for example, if $U_{bulk} < U_{surface}$, then the bulk relaxation should be observed first. In [11] it was explained that the FE appears due to both bulk pinning and surface barriers, thereupon bulk pinning is more important at low temperatures while surface barriers at high temperatures. The goal of this work was to contribute to the understanding of the FE origin in terms of significant influence of both bulk pinning and surface barriers.

*Electronic address: dmitry.a.lotnik@univer.kharkov.ua

II. EXPERIMENT DETAILS AND SAMPLES

Undoped and Ag - doped YBCO bulk single-grain samples were fabricated by a top seeded melt-growth process (TSMG). Oxide powders $YBa_2Cu_3O_7$ + $0.25Y_2O_3$ + addition of Ag_2O in concentration determined by $x = 0.02$ in $YBa_2(Cu_{1-x}Ag_x)_3O_{7-\delta}$ were milled in a friction mill and pressed into cylindrical pellets of 20 mm diameter. A $SmBa_2Cu_3O_7$ type seed with geometrical dimensions 2×2×1 mm^3 was placed in the middle of the top surface of the pellet. The samples were heated in a chamber furnace to a sintering temperature, $T_{sint} = 950°C$, sintered for 24 h and then heated to melting temperature, T_m =1040°C, dwelled for 9 h, cooled to 1000°C and then a YBCO crystal was grown during slow cooling to 950°C. Grown samples were cut in two halves along the {100} plane. The cut surface was grinded on SiC papers and fine polished with alumina powder. The microstructure of the sample was analyzed by an optical microscope in normal and polarized light [12]. The pureness of Ag_2O is 0.005 Wt%. There are {110} type of twins with twin spacing about 200 nm. Twin boundaries are parallel to the c-axis and formed almost 45° angle with the a-axis. Small samples for oxygenation and magnetization measurements were cut from the a - growth sector of the bulks [13] at a distance of 1 mm from the seed (top surface of the pellets). The samples dimensions are shown in Table I.

Two samples, pure crystal (S1) and Ag-doped crystal (S2), were used in the present work. Physical properties of the samples are presented in Table I.

Sample	T_c, K	ΔT_c, K	a(b)×b(a)×c, mm^3	m, mg
S1	90.2-89.8	1.0	2×1.8×0.7	12.2
S2	91.3-91.1	1.5	1.7×1.6×0.8	17.98

Table I: Physical characteristics for samples $YBa_2Cu_3O_{7-\delta}$ (S1) and $YBa_2(Cu_{1-x}Ag_x)_3O_{7-\delta}$ (S2)

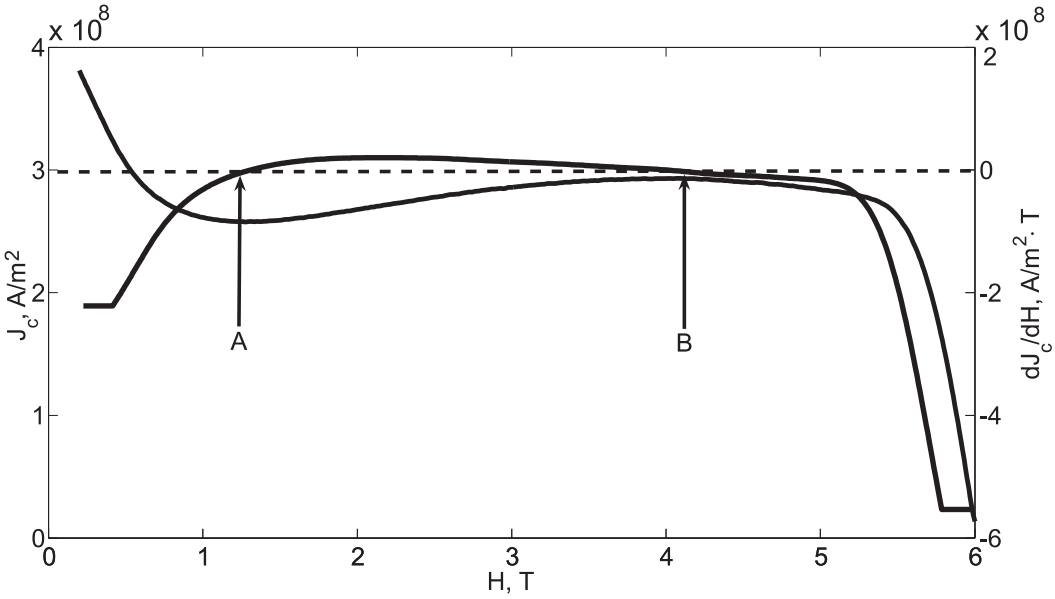

Figure 1: Field dependences of critical current density J_c and derivative dJ_c/dH at temperature T =60 K for sample S1 right after annealing. Points A and B denotes positions of minimum and maximum respectively.

The measurements of isothermal hysteresis loops ($M(H)$ curves) at various temperatures (20 K< T <85 K) were carried out in fields (-6 T< H <6 T) parallel to the c-axis by means of a commercial vibrating sample magnetometer (VSM). The field sweep rate dH/dt was about 0.1 T/min. The relaxation data were measured at each temperature at zero magnetic field (remanent magnetization) during 300 s with $M > 0$ and $M < 0$. To obtain an additional parameter ΔT_c the resistivity $R(T)$ curves were measured on two samples which were obtained from the same single-domain bulks as S1 and S2. Transport measurements were performed using a physical property measurement system (PPMS). The experiment was divided into two steps. $M(H)$ curves were measured: a) right after annealing of samples in oxygen (during 240 hours at 400°C); b) after long-term aging at the room temperature (six months), in which case almost all relaxation processes were finished. The first value for T_c in Table I corresponds to a) and the second value corresponds to b). The magnetic relaxation was measured for each curve in zero magnetic field during 300 s.

III. MODEL TO ANALYZE EXPERIMENTAL DATA

From the measured $M(H)$ curves the critical current density was calculated using the critical state model [14] that have been developed in [15, 16]:

$$J_c = 2\Delta M \frac{\rho}{a^2\,(b - a/3)\,c}, \tag{1}$$

where $\Delta M = M_1(H) - M_2(H)$ ($M_1(H) > 0$, $M_2(H) < 0$ are the values of magnetic moment at field H), ρ is the weight of sample, a, b and c are geometric dimensions of sample ($b \geq a$). Dependences $J_c(H)$ (Fig. 1) were calculated for the field range 0 T $< H <$ 6 T. To obtain the exact position of maximum on $J_c(H)$ curves the derivative dJ_c/dH was calculated for each temperature (see example at Fig. 1). Fig. 1 shows the positions of both minimum (point A) and maximum (point B) on the J vs H curve, where derivative $dJ_c/dH = 0$.

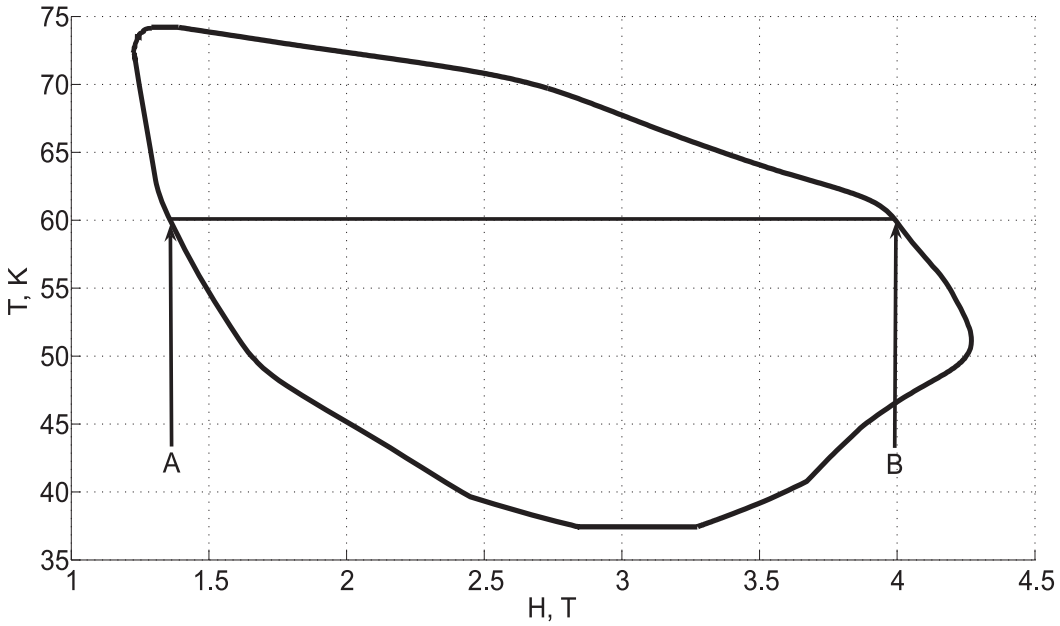

Figure 2: Contour for $dJ_c/dH = 0$ for sample S1 right after annealing. Points A and B coincide with those in Fig. 1

Then the 3D surface T vs H vs dJ_c/dH was obtained. Intermediate curves were defined by the 3rd degree polynomial (spline-function). The contour for $dJ_c/dH = 0$ is shown in Fig. 2. Points A and B correspond to those in Fig. 1. This method is useful to obtain positions of maximum $J_{c,max}$ (or ensemble of points B) not only at given temperatures but also for intermediate temperatures.

IV. RESULTS AND DISCUSSIONS

Fig. 3 shows the zero-field-cooled (ZFC) $M(T)$ curves at certain values of magnetic field (from 0.5 T to 6 T). As one can see magnetization monotonically changes with temperature and no apparent peak is visible on any ZFC $M(T)$ curve. This is characteristic that the FE in $M(H)$ curves cannot be simultaneously observed on a single ZFC $M(T)$ curve, contrasting with the FE caused by the order-disorder vortex matter transition. Hence, this fact can be used as a criterion to distinguish the FE originated from bulk pinning from that induced by the order-disorder vortex matter transition [5–7]. Magnetic relaxation data shows a linear dependence in $M(lnt)$ coordinates (fig. 4). The results for magnetic relaxation are shown in fig. 5.

The total magnetic moment $M = M_{surface} + M_{bulk}$. If surface activation energy $U_{surface}$ is larger than the bulk one, $U_{surface} \gg U_{bulk}$, the rate $R_{bulk} = dM_{bulk}/dlnt \gg dM_{surface}/dlnt$ [10], i.e. $dM/dlnt \approx dM_{bulk}/dlnt$. On the contrary, if $U_{bulk} \gg U_{surface}$ or $R_{surface} \gg R_{bulk}$ then $dM/dlnt \approx dM_{surface}/dlnt$. The crossover between these two regimes manifests itself in the changes of the $M(lnt)$ curve slope.

As one can see (fig. 5) the relaxation rate $R = dM/dlnt$[10] non-monotonically changes with temperature. Temperature range can be divided into 3 parts:

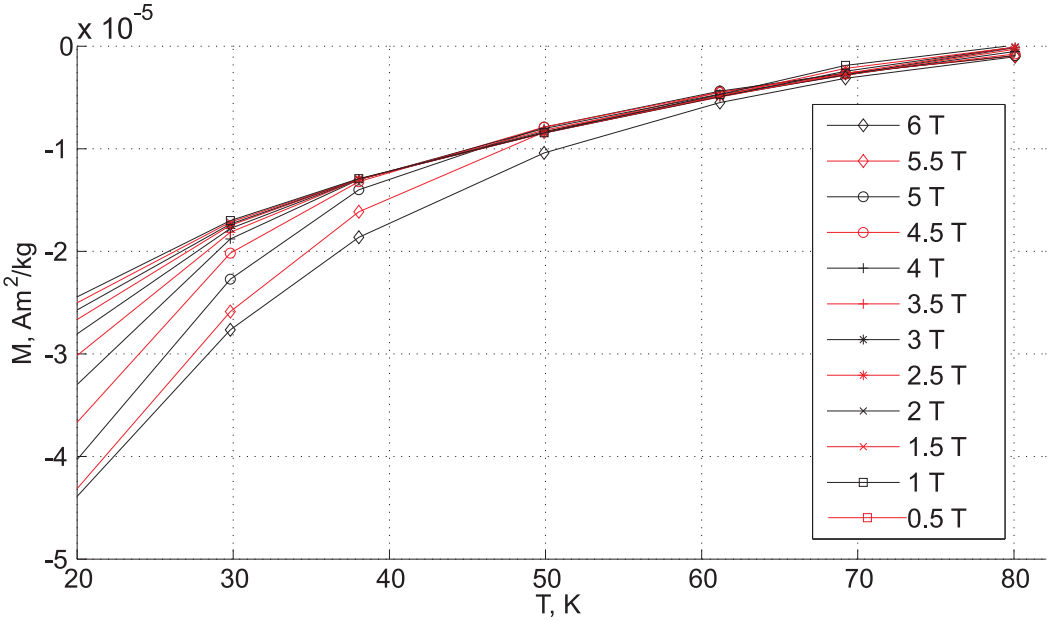

Figure 3: Color online. M(T) curves for the ZFC process in fields from 0.5 T to 6 T for sample S1 six months after annealing

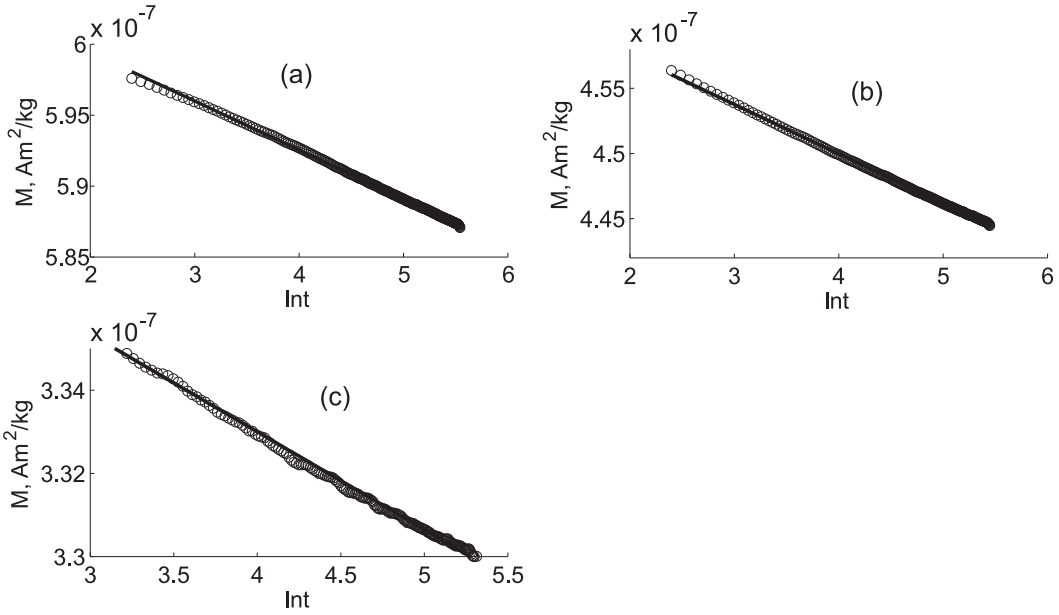

Figure 4: Time dependences of magnetic moment for sample S1 in $M - lnt$ coordinates for low $T/T_c \approx 0.2$ (a), intermediate $T/T_c \approx 0.55$ and high $T/T_c \approx 0.85$ temperature ranges (see text). Circles corresponds to experimental data, solid line corresponds to linear approximation.

1. At low temperatures ($0.2< T/T_c <0.4$) bulk pinning dominates over surface barriers, i.e. the activation energy $U_{bulk} > U_{surface}$ and total relaxation rate R_{total} decreases. The position of minimum of relaxation rate R for Ag-doped crystal shifts to the higher temperatures ($T/T_c = 0.4$ for doping-free sample, $T/T_c = 0.45$ for Ag-doped sample) as compared to doping-free sample. The bulk pinning for the Ag-doped sample is stronger than for the doping-free one due to additional pinning centers, i.e. Ag atoms [17]. That is why relaxation in Ag-doped sample due to $R_{surface}$ dominate to a higher temperatures then in undoped sample.

2. At intermediate temperatures ($0.4 < T/T_c < 0.8$) bulk pinning strongly decreased as compared to surface barriers. This leads to a appreciable decrease of activation energy U_{bulk} and, hence, the relaxation rate R_{bulk}

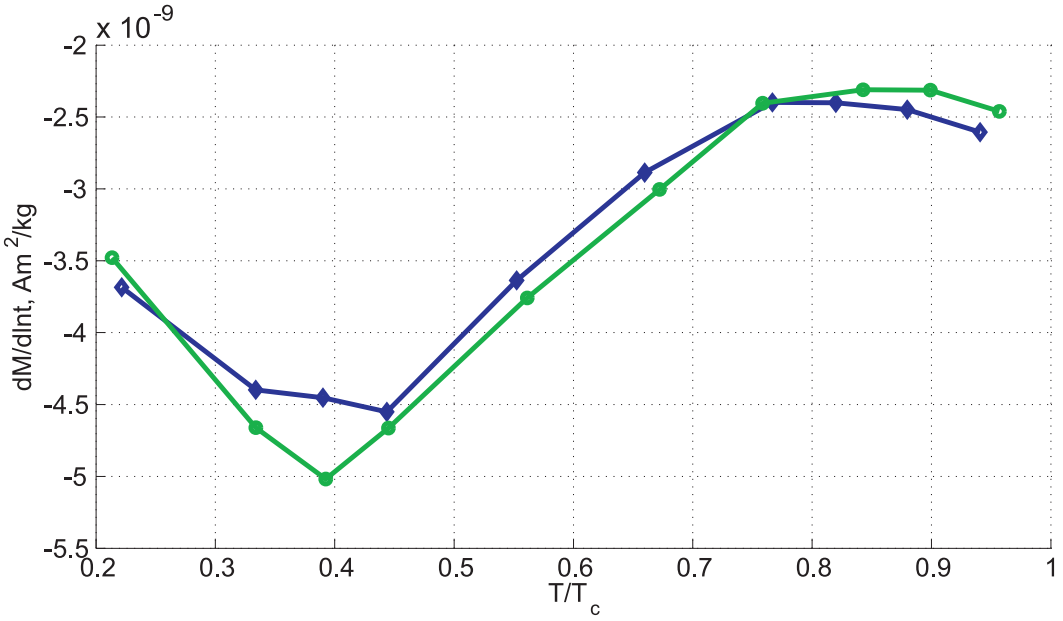

Figure 5: Color online. Temperature dependences of relaxation rate R=dM/dlnt for samples S1 (green) and S2 (blue) six months after annealing

dominates over $R_{surface}$. As a result R_{total} increases. It is significant to note that bulk pinning decreases with increasing temperature and at critical temperature disappears whereas surface barriers still finite.

3. At high temperatures (T/T_c >0.8) R_{total} have plateau. However relaxation rate smoothly decreased. That behavior probably corresponds to significant suppression of bulk pinning near T_c while surface barriers are still finite. Therefore, the value of the captured magnetic flux due to bulk pinning is negligible compared to the $R_{surface}$ and slightly higher than R_{bulk}.

From the model presented in previous section the $H(T)$ dependences of $J_{c,max}$ were obtained (see Fig. 6).

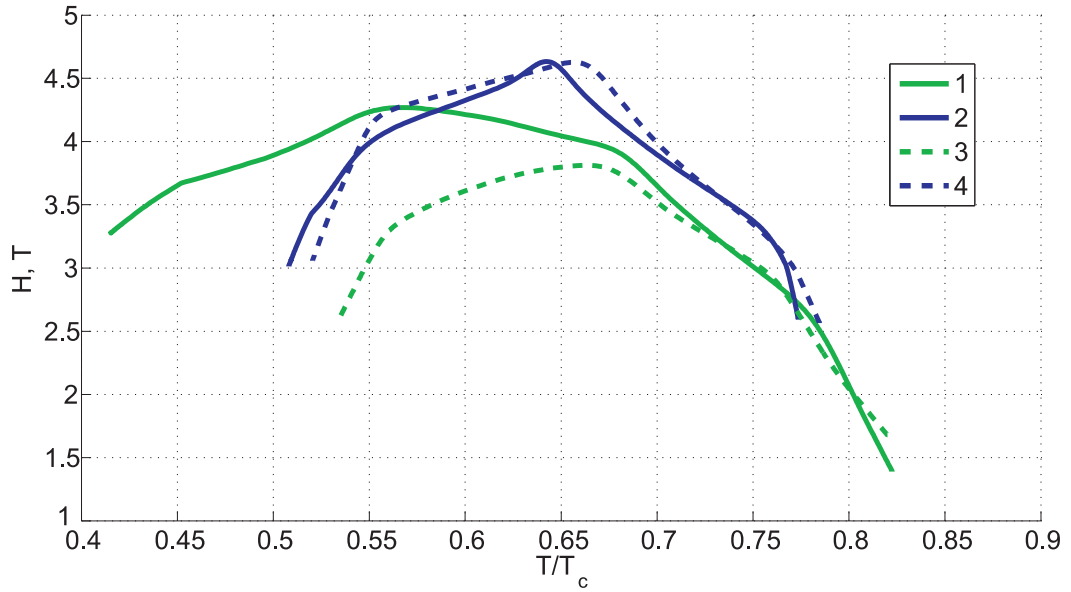

Figure 6: Color online. Temperature-field dependences of $J_{c,max}$-position for samples S1 (green lines) and S2 (blue lines), right after annealing (curves 1,2) and after long-term aging (curves 3,4)

As one can see from Table I the value of the critical temperature T_c for sample S1 changed from 90.2 K to 89.8 K

and for sample S2 from 91.3 K to 91.1 K. This indicates that the optimal oxygen annealing process and aging effects are not caused by changing δ (especially for sample S2). Fig. 6 shows that the position of $J_{c,max}$ significantly changes after long-term aging. The maximum field H_{max} for sample S1 decreases from 4.25 T to 3.8 T and the minimum temperature T_{min} increases from 0.42 to 0.54 (curves 1 and 3 in Fig. 6). Such changes can be induced by the redistribution of pinning centers in the crystal or, in another words, bulk pinning changes during aging. Constancy of the maximum temperature T_{max} for S1 corresponds to the influence of surface barriers at high temperatures. The aging effect for sample S2 is not so significant as for S1. This is related to the presence of considerable mechanical tensions in the sample (large value of an additional parameter ΔT_c =1.5 K) that prevent the redistribution of pinning centers. Larger value of H_{max} (for S2 as compared with S1) corresponds to the presence of additional pinning centers on silver atoms.

A possible reason of the decrease of H_{max} and increase of T_{min} for S1 is the decreasing number of dislocations. In another words, the crystal S1 becomes more homogeneous after aging [18].

V. CONCLUSIONS

In summary, MG YBCO samples were investigated by measuring $M(B)$-curves. On these curves FE was observed in a wide temperature range. The origin of the FE arises for the competition between surface barrier and bulk pinning at intermediate temperatures $0.4 < T/T_c < 0.8$. This is confirmed in a non-monotonically behavior of the relaxation rate R, notably, increase of R at intermediate temperatures due to surface barriers. Bulk pinning influences parameters H_{max} and T_{min} while surface barriers influence T_{max}. Undoped YBCO is characterized by a significant aging effect which is manifested in a considerable change of H_{max} and T_{min}. This corresponds to the change of bulk pinning. For Ag-doped YBCO there are no significant changes in parameters H_{max}, T_{min} and T_{max}. Such difference is caused by the redistribution of pinning centers in undoped YBCO while Ag-doped YBCO is characterized by huge mechanical tensions which prevent redistribution.

Acknowledgments

The work was partly supported by the Slovak Research and Development Agency (No. APVV-0006-07), the Slovak Grant Agency VEGA (No. 1/0159/09) and supported by Project ITMS26220220041 financed through European Regional Development Fund, VEGA project (No. 2/0211/10) and EU network NESPA. The financial support of U.S.Steel - DZ Energetika Košice is acknowledged. One of author (D.L.) is very thankful to the National Scholarship Program of Slovak Republic (SAIA) for the financial support during his stay in Slovakia.

[1] S. Jin, T. H. Tiefel, R. C. Sherwood, M. E. Davis, R. B. van Dover, G. W. Kammiott, R. A. Fastnache and H. D. Keith, Appl. Phys. Lett. **52**, 2074 (1988).
[2] M. Muralidhar, N. Sakai, N. Chikumoto, M. Jirsa, T. Machi, M. Nishiyanma, Y. Wu and M. Murakami, Phys. Rev. Lett. **89**, 237001 (2002).
[3] M. R. Koblischka and M. Murakami, Supercond. Sci. Technol. **13**, 738 (2000).
[4] M. Muralidhar, M. Jirsa, M. Sakai and M. Murakami, Supercond. Sci. Technol. **16**, R1 (2003).
[5] W. Henderson, E. Y. Andrei, M. J. Higgins and S. Bhattacharya, Phys. Rev. Lett. **77**, 2077 (1996).
[6] Y. Paltiel, E. Zeldov, Y. N. Myasoedov, H. Shtrikman, S. Bhattacharya, M. J. Higgins, Z. L. Xiao, E. Y. Andrei, P. L. Gammel and D. J. Bishop, Nature **403**, 398 (2000).
[7] Y. Paltiel, E. Zeldov, Y. N. Myasoedov, M. L. Rappaport, G. Jung, S. Bhattacharya, M. J. Higgins, Z. L. Xiao, E. Y. Andrei, P. L. Gammel, et al., Phys. Rev. Lett. **85**, 3712 (2000).
[8] T. H. Johansen, M. R. Koblischka, H. Bratsberg and P. O. Hetland, Phys. Rev. B **56**, 11273 (1997).
[9] C. P. Bean and J. D. Livingston, Phys. Rev. Lett. **12**, 14 (1964).
[10] L. Burlachkov, Phys. Rev. B **47**, 8056 (1993).
[11] L. Zhang, Q. Qiao, X. B. Xu, Y. L. Jiao, L. Xiao, S. Y. Ding and X. L. Wang, Physica C **445-448**, 236 (2006).
[12] P. Diko, M. Šefciková, M. Kaňuchová and K. Zmorayová, Materials Science and Engineering B **151**, 7 (2008).
[13] P. Diko, Supercond. Sci. Technol. **13**, 1202 (2000).
[14] C. P. Bean, Phys. Rev. Lett. **8**, 14 (1962).
[15] H. P. Wiesinger, F. M. Sauerzopf and H. W. Weber, Physica C **203**, 121 (1992).
[16] M. Jirsa, L. Pust, D. Dlouhy and M. R. Koblishka, Phys. Rev. B **55**, 3276 (1997).
[17] T. Nakashima, Y. Ishii, T. Katayama, H. Ogino, S. Horii, J. Shimoyama and K. Kishio, J. Phys.: Conf. Ser. **97**, 012007 (2008).
[18] H. Küpfer, Th. Wolf, C. Lessing, A. A. Zhukov, X. Lançon, R. Meier-Hirmer, W. Schauer and H. Wüfl, Phys. Rev. B **58**, 2886 (1998).